Correlation and symmetry effects in transport through an artificial molecule

F. Ramírez*
Posgrado en Física de Materiales, Centro de Investigación Científica y de Educación Superior de Ensenada, Ensenada, Baja California, Mexico

E. Cota
Centro de Ciencias de la Materia Condensada-UNAM, Ensenada, Baja California, Mexico

S. E. Ulloa
Department of Physics and Astronomy and Condensed Matter and Surface Sciences Program, Ohio University, Athens, Ohio 45701-2979
(Received 26 August 1998)

Spectral weights and current-voltage characteristics of an artificial diatomic molecule are calculated, considering cases where the dots connected in series are in general different. The spectral weights allow us to understand the effects of correlations, their connection with selection rules for transport, and the role of excited states in the experimental conductance spectra of these coupled double dot systems (DDS). An extended Hubbard Hamiltonian with varying interdot tunneling strength is used as a model, incorporating quantum confinement in the DDS, interdot tunneling as well as intra- and interdot Coulomb interactions. We find that interdot tunneling values determine to a great extent the resulting eigenstates and corresponding spectral weights. Details of the state correlations strongly suppress most of the possible conduction channels, giving rise to effective selection rules for conductance through the molecule. Most states are found to make insignificant contributions to the total current for finite biases. We find also that the symmetry of the structure is reflected in the *I-V* characteristics, and is in qualitative agreement with experiment. [S0163-1829(99)07707-3]

I. INTRODUCTION

A semiconductor quantum dot or ''artificial atom'' is an electronic device defined on the nanometer scale.[1,2] This system usually arises when a homogeneous two-dimensional electron gas (2DEG) generated at the interface between layers of semiconductor structures is laterally confined by electrostatic, mechanical, or other means. An artificial atom is characterized by a strong quantization of the electronic motion in all three spatial dimensions. This means that the spectrum of the electrons is discrete with separation between levels given by a characteristic value, Δ. On the other hand, the extremely low capacitance (both self and mutual) achieved in these nanostructure systems, due to the small sizes and compact geometries of the arrangements, produce a relatively large charging energy of $U=e^2/C\simeq 1$ meV. In most semiconductor structures in this regime, one finds typically that $U>\Delta$, frequently differing by an order of magnitude or more.

In a typical ''lateral'' transport structure,[3] which consists of a quantum dot coupled via tunnel barriers to two reservoirs (source and drain) and a back gate, the number of electrons can be controlled at will, starting from a small number of electrons (or none) in the dot. The charging of the *N*-electron atom with an additional single electron can be done by changing the back gate voltage, as it controls the depth of the local potential well holding the electrons. The charging takes place when the chemical potential of the emitter electrode equals the ''local'' chemical potential of the atom, by providing enough energy for the system to receive a particle. Since a large energy U is required, this gives rise to the *Coulomb blockade* (CB) of transport whenever this energetic condition is not met. The CB is in fact the mechanism for the surprisingly strict control of the charge in the quantum dots, and their denomination as artificial atoms with a well-defined number of electrons at a given set of gate voltages. As a consequence of CB, only one electron at a time can tunnel into the quantum dot for high or wide tunneling barriers, and one observes oscillations of the differential conductance as a function of the back gate voltage, which controls the equilibrium charge of the dot, every time the electron population in the dot changes.[4–6] This in-plane geometry has been explored extensively both experimentally and theoretically.

In a different geometry, an ingenious device that uses a *capacitor* where electrons tunnel between a metallic layer and discrete quantum levels of the confined structure has been studied recently by several groups.[2,7] This sensitive device monitors small capacitance peaks as a function of voltage across the structure every time an electron tunnels into the dot. This method of single-electron capacitance spectroscopy has allowed researchers to monitor the intricate behavior of the many-particle states produced as function of external magnetic fields.[7] Other interesting techniques used to investigate properties of artificial atoms include far-infrared spectroscopy,[8] which explores excitations of these artificial atoms, and recent ''vertical'' transport experiments in novel gated multiquantum well structures.[9,10] Together, these experimental probes provide fascinating insights into the properties of these artificial atoms and molecules, in a similar way to what atomic and molecular physics yield, although the different energies and variable electron number are un-

like anything possible in those systems.

The conductance in transport spectroscopy through a well-defined artificial atom is strongly affected by the Coulomb blockade, as described above,[11] and is a clear manifestation of charge quantization. Notice that when the voltage difference between the source-drain leads is small, one is in the linear-response regime. Here, one can see the collection of differential conductance peaks in terms of the so-called *addition spectrum*, i.e., the series of energy values required to add one electron to the system. This is given by the chemical potential in the leads (and equal to one another in this linear regime), $\mu_N \equiv E_{N,1} - E_{N-1,1}$, where $E_{N,1}$ is the ground-state energy of the N-electron artificial atom. As the back gate (or some other neighboring gate) voltage is shifted, it produces successive conductance peaks in the transport experiment.[12] Therefore, one can say that the linear regime provides a direct measure of the ground states of the system.

On the other hand, in the *nonlinear* transport regime, at finite drain-source bias voltages, additional conductance peaks are observed, which reflect the presence and nature of the excited states of the artificial atoms for a given particle number.[13–15] McEuen *et al.*[16] have realized transport spectroscopy on single dots and carefully analyzed the role of excited states versus source-drain bias and magnetic fields. In the case of single quantum dots, exhaustive studies of the excited states pointed out that a large number of the available states do not contribute to the conductance, signaling the existence of selection rules *for transport*. In fact, a number of theoretical works demonstrated that indeed unusual selection rules are required to account for the observed suppression of the fine structure. These selection rules appear due to strong correlations in the electron eigenstates and corresponding eigenfunctions.[17–19] The appearance of strict spin selection rules and/or those related to the orbital motion have been associated with the many-particle nature of these states and provide a natural explanation of the experimental data.

Our goal in this paper is to understand how discrete energy levels, electron-electron interactions and symmetry affect the spectrum in an artificial diatomic molecule (coupled quantum dots), and how this is reflected in the linear and nonlinear transport characteristics. This will be especially important for the strongly-correlated few-electron regime, as it is widely expected that increasing carrier number or concentration ends up making the quantum dot not too dissimilar from a classical polarizable droplet (at zero magnetic field). Arrays of quantum dots have been modeled to study the addition spectra and conductance.[20–22] Notice also that transport measurements have been reported for arrays of two or more dots connected in different geometries. These artificial molecules have conductance peaks that split as a function of interdot interaction,[23,24] and show interesting charging diagrams, be it in a series,[24,25] or parallel connection.[26,27] Linear and nonlinear transport experiments conducted on two coupled dots in series indicate that as interdot tunneling is turned on, this interaction allows charge to distribute throughout the system and controls the evolution from a two-dot system to a larger dot.[25,28,29] Beautiful direct evidence of a fully developed coherent-resonant ''molecular state'' (in terms of the classical ''symmetric/antisymmetric'' or ''bonding/antibonding'' quantum mechanical states) has recently been presented by Blick *et al.*[25,30] These authors have focused on the study of a coherent molecular state than can be found in the charging diagram of the double dot system. This charging diagram is constructed by varying ''top'' and ''back'' gate voltages in the linear transport regime, and ''triple points'' were identified where the device could be used as an electron pump.

The evolution of the differential conductance as a function of interdot tunneling for the series-connection has been treated theoretically for a symmetric double dot system by Kotlyar *et al.*,[31] combining a step-well model for the confinement potential of the system used in Ref. 29. They used a Mott-Hubbard model to describe the electronic interactions, and obtained excellent qualitative agreement with the measured currents in the nonlinear regime.

Here we study an artificial diatomic molecule that is a simple coupled array of two quantum dots connected in series. We consider the general case where the two dots are not identical (both the ''symmetric'' and ''asymmetric'' cases), similar to the system in Ref. 25. We model the system with an extended Hubbard Hamiltonian, which takes fully into account the interaction between quantum dots in a real system: interdot tunneling interaction defined in a typical lateral structure by tunable gates, and the intra- and interdot Coulomb repulsion. We apply the analysis of the spectral weights (''overlaps'') following Ref. 19, for the few-electron eigenstates of the quantum system. The Hamiltonian allows us to calculate exactly the entire energy spectrum of this multiparticle system by numerical diagonalization, as well as the full eigenfunctions of the system. The current through the molecule is determined to a great extent by the spectral weights of the states involved in the transitions in the dots, which also describe the electronic correlations in the system. Regarding only sequential tunneling, the total current through the artificial molecule incident from the left reservoir can be written explicitly as (with a similar expression for transport through the right barrier)[32]

$$I = -e \sum_{\alpha\alpha'} \tilde{\Gamma}^{L}_{\alpha\alpha'} [P((N-1),\alpha') f^{L}_{\alpha\alpha'} - P(N,\alpha)(1 - f^{L}_{\alpha\alpha'})]. \tag{1}$$

The Fermi distribution function $f^{L}_{\alpha\alpha'} = f_{FD}(\Delta E_{\alpha\alpha'} - \mu_L)$, characterizes the occupation of the electron levels in the left reservoir (with chemical potential μ_L). Here the resonant energy $\Delta E_{\alpha\alpha'} = E_{N,\alpha} - E_{N-1,\alpha'}$, is the difference between the energy of an N-particle state α, $|N,\alpha\rangle$ and an $(N-1)$-particle state α', $|N-1,\alpha'\rangle$. The probability $P(N,\alpha)$ of finding the quantum molecule in the N-particle state α will deviate from its equilibrium value for a given drain-source voltage. Its dependence on the tunneling rate $\tilde{\Gamma}^{L}_{\alpha\alpha'}$ is well described by kinetic equations.[12,32,33] The corresponding tunneling rate $\tilde{\Gamma}^{L}_{\alpha\alpha'}$ depends on the single-electron tunneling rate Γ^{L}_{n} for an electron traversing the system in the state n, and the details of the multiparticle states. Since the energy (or n) dependence of Γ^{L}_{n} is weak and/or monotonic, we further conclude that the tunneling rate is dominated by the intrinsic spectral weight so that $\tilde{\Gamma}^{L}_{\alpha\alpha'} = \gamma^{L} S^{L}_{\alpha\alpha'}$, where γ^{L} is a smoothly energy-dependent single-particle tunneling rate, and the overlap or spectral weight is

$$S^{L}_{\alpha\alpha'} = \sum_{n \in L} |\langle N,\alpha|C^{\dagger}_{n}|N-1,\alpha'\rangle|^{2}. \quad (2)$$

This quantity describes the correlations in the system, and its contribution to the current (I-V) characteristics proves to be dominant in determining the salient features measurable in experiments. The spectral weights govern the tunneling probability because they describe the overlap between the N-electron state α, and the compound state built by an incoming electron with quantum number(s) n added to the $(N-1)$-electron state α'. For a system of uncorrelated electrons this overlap will be either one or zero between any two states, by definition, in an orthogonal basis. However, electron correlations result in overlaps much less than unity, as the correlations built into the states severely limit the possible ''conduction channels,'' and the tunneling probability is consequently reduced considerably.

Our study here of the overlap matrix elements not only gives us insights into the physical process behind the selection rules, but also allows us to explore the general properties of the current characteristics to be measured in these systems. The aim of this work is to investigate the effect of interdot tunneling interaction and interdot Coulomb repulsion on the spectral weights and current-voltage characteristics through a double dot system (DDS). Given recent experiments with dots with markedly different sizes, we also study the effect of this structural asymmetry on the state correlations and ensuing transport properties. This asymmetry, typically implemented with top gate arrangements, provides an additional parameter, which allows exploration of the correlations in the system.

In the Hubbard approach we use here, we find that the interdot tunneling interaction has a direct effect on the spectral weights and I-V characteristics, since it controls the possible delocalization of the wave function and effectively regulates the correlation of the different states. The spectral weights critically depend on the number of electrons N because interactions change every time an electron enters the system, and the number of channels increases rapidly with N. We find also that the structural asymmetry is most evident in the I-V characteristics for small interdot tunneling, but present even for relatively well-connected dots in the DDS.

II. MODEL

We use the extended Hubbard Hamiltonian,

$$\hat{H} = \sum_{j\alpha} \epsilon_{j\alpha}\hat{C}^{\dagger}_{j\alpha}\hat{C}_{j\alpha} - \sum_{\alpha\beta ij} t_{\alpha\beta}\hat{C}^{\dagger}_{i\alpha}\hat{C}_{j\beta} + \frac{1}{2}\sum_{j} U_{j}\hat{n}_{j}(\hat{n}_{j}-1) + \sum_{i>j} V_{ij}\hat{n}_{i}\hat{n}_{j}, \quad (3)$$

where the parameters take into account the different types of interactions. Here $C^{\dagger}_{j\alpha}$ and $\hat{C}_{j\alpha}$ are creation and annihilation operators, $\hat{n}_{j}$ is the electron number operator at site j, and $\epsilon_{j\alpha}$ are the confined energy levels of the αth state in the jth quantum dot; these levels are assumed to be equally spaced with separation Δ_{j} (as appropriate for a local harmonic oscillator confinement potential which should be a good description of typical ''lateral'' dots). U_{j} is the on-site Coulomb repulsion for the jth quantum dot, V_{ij} is the interdot repulsion, and $t_{\alpha\beta}$ is the tunneling matrix element between the single-particle states α and β in the respective neighboring dots. Kotlyar and co-workers have presented a parametrization of the classical capacitance matrix elements in terms of the Hubbard Hamiltonian quantities.[31] Some of the details will change from their square-well potential to our harmonic oscillators, and these depend on gate geometries and other structural features. In either case, one would obtain intrinsic Hubbard parameters with characteristic values of $U_{j} \simeq 1$ meV, and $U_{j} \gg V_{ij} \simeq 0.1$ meV, in the typical GaAs structures used in experiments.

The parameter $t_{\alpha\beta}$ is perhaps the most sensitive to the specific gate implementation and applied gate voltages. In fact, the interdot barrier transparency has been used superbly to control the overall interdot conductance in the experiments of Crouch *et al.*,[29] and Blick *et al.*,[25] to name a few groups.[34] These tunneling parameters effectively control the correlations between states in the DDS, by limiting the wave function overlaps. It is the well-known competition of this tunneling with the Coulomb interactions that determine the details of correlations in the states.[20]

The specific values of the tunneling matrix elements depend on how the interdot barrier is formed and modeled, so that $t_{\alpha\beta}$ can be assumed to be given by a Gaussian distribution (in energy difference) that simulates the expected decreasing coupling between levels that are not resonant or nearly so.[35] In order to evaluate the effect of the interdot coupling differences, we compare two different regimes. On the one hand, the case of a diagonal matrix $t_{\alpha\beta} = t\delta_{\alpha\beta}$ describes tunneling between aligned states only (likely the case for high/wide barriers). On the other hand, the case of a constant distribution given by $t_{\alpha\beta} = t$, where tunneling between all states is allowed, give us two opposite coupling regimes. This latter case can be used to describe the strong tunneling regime resulting when the interdot barrier is low and/or narrow. For a dot of diameter $d = 100$ nm in a $GaAs/Al_{x}Ga_{1-x}As$ heterostructure, the charging energy $U \simeq 1$ meV, which greatly exceeds the thermal energy $k_{B}T$ at the characteristic dilution refrigerator temperatures of $\simeq 0.1$ K, so that it is safe to assume that these devices work in the quantum regime, $k_{B}T < t < \Delta_{j} < U$. In this description, we may use spin orbitals and the spin overlap contribution can be considered,[18] especially for finite magnetic fields, but we choose to model the artificial molecule as a system of spinless fermions for simplicity. This restriction can be clearly relaxed, but given the typically much smaller Zeeman splitting, we do not expect that our conclusions would be drastically changed at these temperatures and for typical structures.

The procedure we follow is to solve the extended Hubbard Hamiltonian (3) in the particle number representation by direct diagonalization to obtain the eigenvalues and eigenvectors for the system with N electrons, and use Eq. (2) to calculate the spectral weights. The system wave functions are expressed in the local orbital representation, and we find then how the creation operator $C^{\dagger}_{n}$ transforms the state $|N-1,\alpha'\rangle$, for example. Any of these states is a linear combination of local orbitals with coefficients (probability amplitudes) that describe the state fully. As the electron enters the DDS, it delocalizes into a complex molecular electronic state

$C_n^\dagger|N-1,\alpha'\rangle$. The projection of this new state of the molecule over the state $|N,\alpha\rangle$ gives us information about that delocalization, which is a product of the interplay between the hopping reducing confinement and the Coulomb interaction, which effectively suppresses tunneling. The analogy with chemistry, describing our system as a covalently bonded artificial molecule, gives us a deeper insight into the processes taking place here.[25] Notice, however, that the repeated and sequential particle addition to the molecule via transport through the leads is clearly unlike any process in atomic or molecular physics, as mentioned in the Introduction.

We find that in the strong tunneling and interacting regime (highly correlated system) most of the spectral weights take values near zero and only some specific channels dominate the spectra as occurs for single dots.[19] The consequences of these strong and effective selection rules for the current through the system are calculated using Eq. (1), or the equivalent symmetrized expression (taking into account the tunneling from the left and the right explicitly)

$$I=\frac{e}{2}\sum_{\alpha\alpha'} P(N-1,\alpha')[\tilde{\Gamma}^R_{\alpha\alpha'}f^R_{\alpha\alpha'}-\tilde{\Gamma}^L_{\alpha\alpha'}f^L_{\alpha\alpha'}] + P(N,\alpha)[(1-f^L_{\alpha\alpha'})\tilde{\Gamma}^L_{\alpha\alpha'}-(1-f^R_{\alpha\alpha'})\tilde{\Gamma}^R_{\alpha\alpha'}], \quad (4)$$

which we use in all calculations below. In this equation, the factors $P(N,\alpha)$ are the probabilities of having the system with N electrons in the state α. These can be obtained from the solution of rate equations, as discussed in the literature,[12] for an accurate evaluation of all the limiting rates during the conduction process. Here, we assume for simplicity, that these probabilities are well described by a superposition of two equilibrium distribution functions determined by the chemical potentials at each reservoir, so that $P=(P_R+P_L)/2$, where $P_{L/R}=\exp[-\beta(E_{N,\alpha}-N\mu_{L/R})]/Z(\mu_{L/R})$. Here, Z is the Gibbs distribution function for each of the reservoirs at chemical potential μ_L and μ_R. Although this independent ''feeding'' of the DDS by each reservoir is only an approximation, it turns out that it is not too far from the full solution of the rate equations, except for large biases, and whenever the overlaps change drastically with energy.[33] In this expression, we have also added the appropriate bias and gate voltage dependence to the energy spectrum, so that $E_{N,\alpha}=E^0_{N,\alpha}-eN(c_GV_G+c_BV_{DS})$, where $E^0_{N,\alpha}$ are the eigenvalues of the Hamiltonian (3), and the constants c_G and c_B are proportional to the capacitance between the dots and the gates defining the voltages. As a typical example of nonidentical dots, we take a constant value of $\lambda=c_B/c_G=2/3$, while one would expect $\lambda=1/2$ in a symmetric structure.

As a finite bias V_{DS} is applied to the DDS, one is in the nonlinear transport regime, and the left and right reservoirs are offset from each other by $eV_{DS}=\mu_L-\mu_R$. When sufficiently large bias voltage V_{DS} is applied, new channels are open for electron conduction and the overlaps measure the probability for single electron tunneling through each channel. Since the spectral weights $S_{\alpha\alpha'}$ provide the information

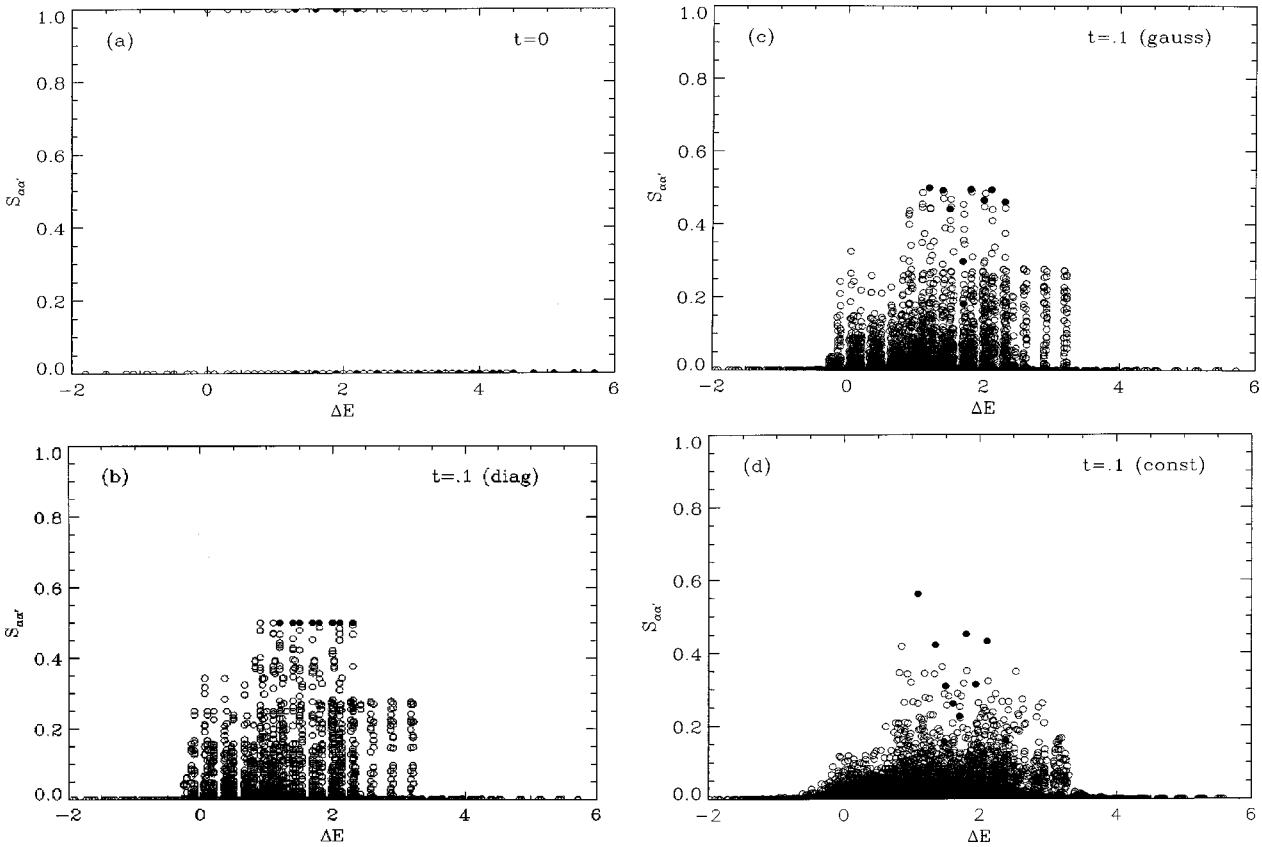

FIG. 1. Spectral weights as a function of the energy difference $\Delta E_{\alpha\alpha'}$ between states involved in the transition $N{:}2\rightarrow3$, for different interdot tunneling models: (a) $t=0$, (b) diagonal $t_{\alpha\alpha'}=t\delta_{\alpha\alpha'}$, (c) Gaussian, (d) constant $t_{\alpha\alpha'}=t$. Filled circles represent channels $(\alpha,\alpha'=1)$ for all α. Symmetric DDS case. $U_1=U_2=U$; $\Delta_1=\Delta_2=0.3U$.

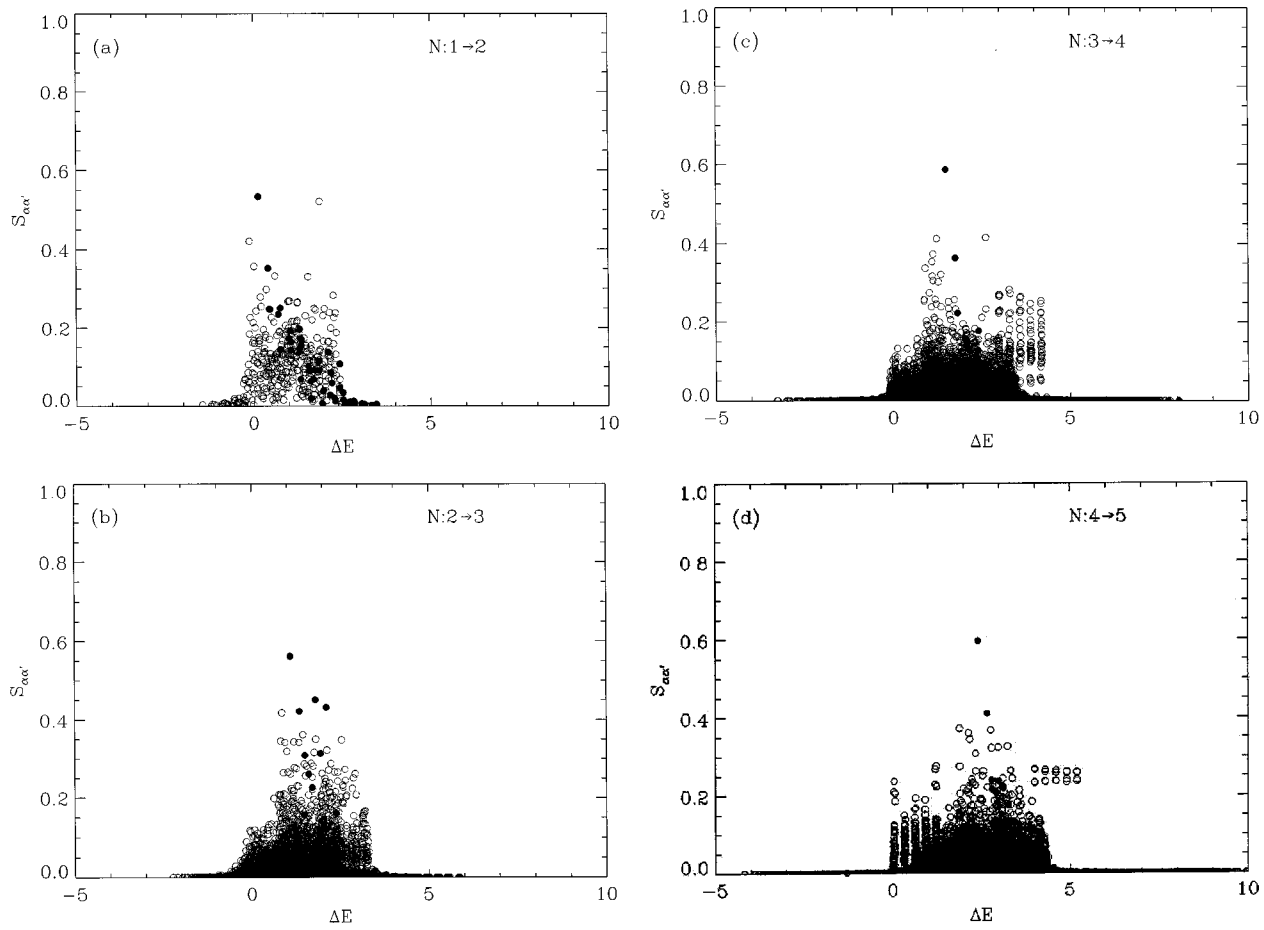

FIG. 2. Effect of number of electrons N on spectral weights in the constant regime ($t_{\alpha\beta}=0.1$). Symmetric molecule case.

for the current-voltage characteristics, and in the nonlinear regime the energy scale of interest is $\Delta E_{\alpha\alpha'} \propto eV_{DS}$, we analyze these weights over varying energy intervals $\Delta E_{\alpha\alpha'}$ to identify the channels (α,α') that contribute to the current in that interval. Thus, we have the possibility of identifying the particular channel that contributes to the current at a given voltage and proceed to compare with the experimental results. In this regime, to calculate the current with Eq. (4), we must take into account all channels in the appropriate energy window, but our calculation shows that only a rather small number of them contribute significantly to the transport rate via Eq. (2).

III. RESULTS AND DISCUSSION

In what follows, we will measure all energy parameters in the Hamiltonian in terms of the local repulsion $U \simeq 1$ meV, characteristic of typical systems. To provide contrast for the different regimes, we consider here two cases: (a) the case of symmetric quantum dots, where the harmonic-oscillator level spacing and intradot Coulomb interaction are the same in each site, i.e., $U_1=U_2=1$ and $\Delta_1=\Delta_2=0.3$; (b) the ''asymmetric'' case, where the two quantum dots in the molecule are not the same, and the structural parameters are different. As an example, we take $\Delta_1=0.3,\Delta_2=0.2$ and $U_1=1,U_2=0.8$, corresponding to a larger dot with the index 2. Notice that since the dot 2 is assumed larger (with size L_2), both the harmonic confinement ($\propto L_2^{-2}$), and the local repulsion term ($\propto L_2^{-1}$) yield smaller values than for the small dot in site 1. We should also mention that inclusion of a finite and reasonable interdot interaction V_{12} ($\lesssim U/10$) yields rather small energy shifts in the energy level spectrum (similar to a slight rescaling of the value of U), and negligible effects in the spectral weights, in general. In what follows, and without loss of generality, we present results with $V_{12}=0$.

A. Spectral weights

In Fig. 1, we show results for the spectral weights $S_{\alpha\alpha'}$ for the *symmetric* double dot system as a function of the energy difference $\Delta E_{\alpha\alpha'}$ between the states involved in the transition, corresponding to the case where the number of electrons goes from $N=2$ to $N=3$ for different intensities of tunneling coupling. In all the figures, we identify with filled circles the channels $(\alpha,1')$, that represent transitions between *all* possible states $|N,\alpha\rangle$ of N electrons and the *ground* state $|N-1,1'\rangle$ of $(N-1)$ electrons; empty circles denote all other pairs. Figure 1(a) illustrates that without tunneling ($t=0$) the electrons in the system are totally uncorrelated and, correspondingly, the overlaps are either zero or one. Figures 1(b) and 1(c) reveal the connection between electronic correlations and tunneling measured by $S_{\alpha\alpha'}$ in the weak tunneling regime, for different coupling models. In Fig. 1(b) we

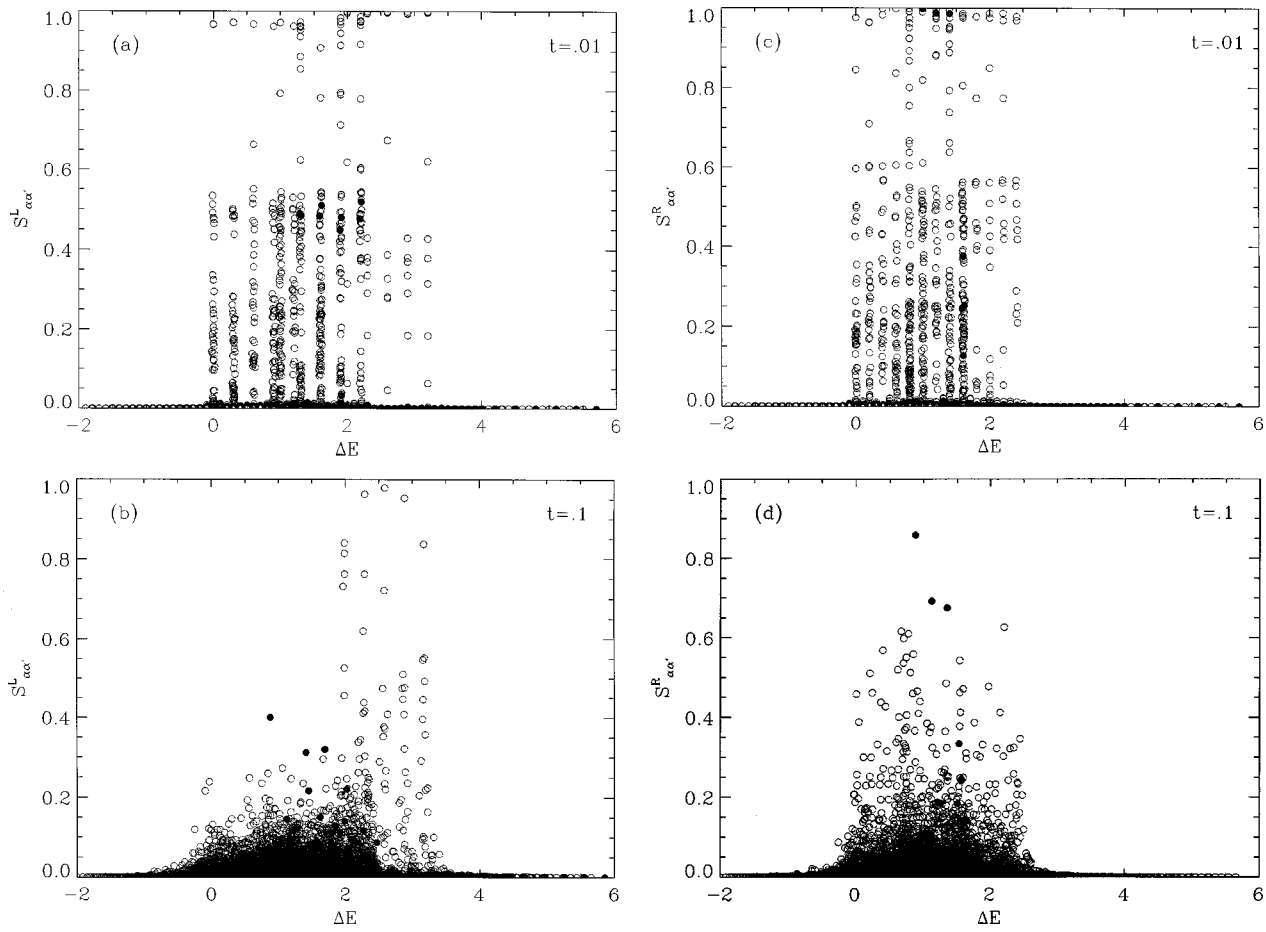

FIG. 3. Spectral weights in asymmetric DDS case, with $U_1=1$; $U_2=0.8$; $\Delta_1=0.3$; and $\Delta_2=0.2$. Electrons incident from left [(a) and (b)] or right [(c) and (d)], with t values as shown, for the $N:2\rightarrow3$ transition.

use the diagonal tunneling matrix $t_{\alpha\beta}=t\delta_{\alpha,\beta}$ with $t=0.1$. As t is gradually increased one obtains progressively smaller values of $S_{\alpha\alpha'}$ for most state pairs, and only a chosen few are nonzero (notice large number of circles on the horizontal axis). This general behavior is also obtained for different $t_{\alpha\beta}$-matrix coupling, even if the details of the suppressed transition pairs change somewhat. In Fig. 1(c), we couple all single-particle states between dots with an energy-dependent Gaussian distribution with a maximum at $t=0.1$ on resonance. Notice the rather similar behavior to Fig. 1(b). The extreme regime of strong coupling is explored by taking a constant distribution $t_{\alpha\beta}=t$. To compare results we use again $t=0.1$, and see in Fig. 1(d) that a signature of this most correlated system is a strong suppression of the weights $S_{\alpha\alpha'}$, and a clear prevalence of the transitions involving the ground-states [highest spectral weights occur for the lowest energy-filled circles in Fig. 1(d)], and low-lying excitations of the DDS. As most of the channels have low spectral weights, their contribution to the current will be small in a transport experiment, according with Eq. (2). Only the few channels with large spectral weights would give origin to discernible peaks in the differential conductance traces, as we will see in the next section. In particular, in Fig. 1(d), the largest contribution comes from the transition involving the ground states from $N=2$ to $N=3$, suggesting that nonlinear conductance features would be quite small at finite bias. This observation is verified later when we actually calculate I-V diagrams and is in qualitative agreement with experiments.[29]

Figure 2 presents typical results for overlaps in the symmetric DDS case for the sequential addition of electrons, from $N=1$ to $N=5$. The number of particles in the system obviously modifies the interactions and, as a consequence, the eigenfunctions generate different spectral weights for each channel with the addition of electrons. We use here $t=0.1$ for all pairs in this system, a strongly correlated case. We observe that the correlations in the artificial molecule are different for the same interval $\Delta E\propto V_{DS}$ for different N, since interactions readjust every time an electron enters the system. The symmetry of the artificial molecule leaves as signature on the spectral weights that the channel $(1,1')$ ends up having always the maximum overlap. The results are different in the asymmetric case. As will be shown below, there are many channels (α,α'), that are directly related to the excitation spectra of the artificial molecule, which provide major contributions via large values of the overlaps.

If we calculate the spectral weights for an asymmetric molecule, we observe the effects of the dot asymmetry for different values of tunneling amplitude. For example, we show in Figs. 3(a) and 3(b) spectral weights $S^L_{\alpha\alpha'}$ for an electron that enters the system from the left in the transition $N=2\rightarrow3$. Figures 3(c) and 3(d) show the corresponding re-

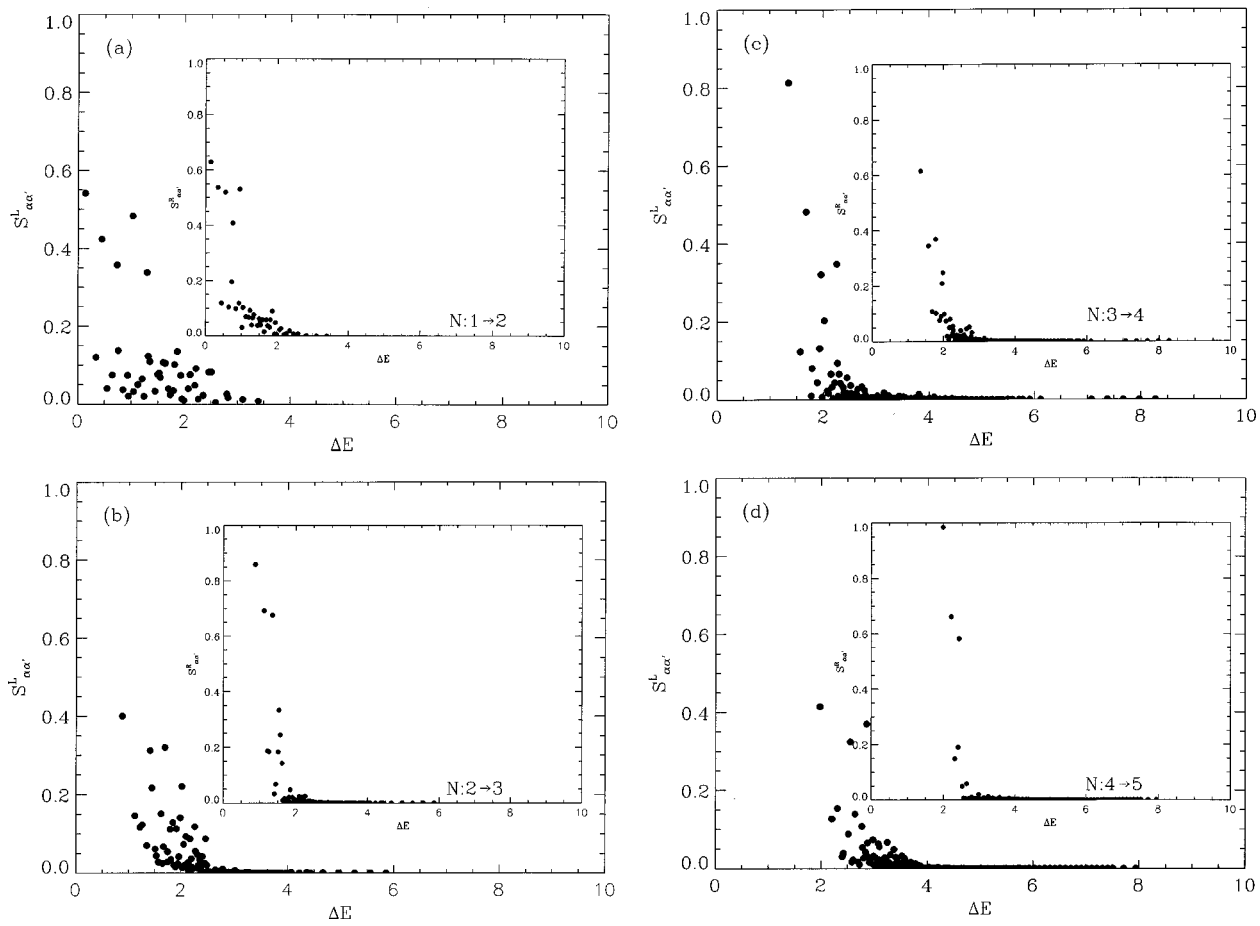

FIG. 4. Spectral weights for left incidence for transitions involving the $(N-1)$-particle *ground state*, for $t=0.1$ in the constant regime and $V=0$. Insets show results for incidence from right.

sults for an electron incident from the right, $S^R_{\alpha\alpha'}$. For the same channels in the same interval ΔE, we obtain in general that $S^R_{\alpha\alpha'} \neq S^L_{\alpha\alpha'}$, as one would expect that the single-particle level asymmetry would carry over to the many-particle states. The overall reduction of the overlaps is evident when t increases, as one electron is added to the system from either left or right. At the same time, we notice a big difference with the symmetric molecule. In the asymmetric case many channels corresponding to transitions between excited states have large overlaps even in the strong tunneling regime, and *even larger* than the $(1,1')$ ground-state transitions for $S^L_{\alpha\alpha'}$ in Fig. 3(b).

Increasing the number of electrons sequentially in the asymmetric case gives the values of the overlaps shown in Fig. 4 for incidence from the left (emitter side for positive V_{DS}). Here, only the contribution from transitions $(\alpha,1')$ are shown (from $E^0_{N-1,1}$ to $E^0_{N,\alpha}$). In the insets, the corresponding overlaps for incidence from the right are shown. In each case, the largest contribution comes from the transition between ground states, and is larger for incidence from the right (left) for transitions from even (odd) to odd (even) N, as expected from the asymmetry considered (larger dot on the right). These transitions involve states that are weighted predominantly on either of the dots, increasing the overlap that comes from a given side and decreasing the other.

The previous analysis illustrates two characteristics of the overlaps. First, they provide selection rules in transport spectroscopy that allow us to explain why the flow of current from the left can be lower or larger for a particular channel as discussed above. The important point is that for any channel in question, we can analyze the calculation and offer an explanation of their contribution to the current. The second point is closely related with the physical process of tunneling. This coupling mixes single-electron states and builds up a molecular state where electrons are correlated. Thus, many electron wave functions of the artificial molecule contain information about ''bonds'' between quantum dots. Tunneling provides a kind of bonding interaction and, as described, this affects the spectral weights in a nontrivial way. In the local-orbital approximation, we can understand that upon operating with the creation operator $C^\dagger_n$, we create an N-particle state $C^\dagger_n|N-1,\alpha'\rangle$, which is in general not one of the eigenstates of the system $|N,\alpha\rangle$ but is rather represented as a linear combination of basis vectors in the N-particle Hilbert space. If there is a dominating $(N-1)$-particle state in a given spectral weight, say the jth state, the overlap will be given by $S_{\alpha,\alpha'}(n) \simeq |\lambda_j|^2 |\mu_k|^2$. Here, $|\lambda_j|^2$ is the probability that the system with $(N-1)$ electrons is in the jth basis state. In a similar way, $|\mu_k|^2$ represents the probability that the artificial molecule occupies the kth basis state with N electrons. If we assume that both states correspond to maximum

(or minimum) probability, this qualitative simplification gives us another approach to explain high or low spectral weights in terms of probabilities associated with basis states. For example, we can explain the values of overlaps for channel $(1,1')$ in Fig. 1(b) this way. We calculate the spectral weight and obtain $|\lambda_{1'}|^2=0.9997$ for an electron incoming from left or right. The operation $C_1^\dagger|N-1,1'\rangle$ gives a vector that is projected over the ground state $|N,1\rangle$. This state has a maximum occupation probability $|\mu_1|^2=0.4984$, so that the overlap is given by $|\lambda_{1'}|^2|\mu_1|^2\simeq 0.5$. The exact value obtained from Eq. (2) is 0.4996. Notice that this simple analysis gets complicated rather quickly as t increases, since many more occupation probabilities $|\lambda_j|^2$ need to be considered to build up the given state $|N-1,\alpha'\rangle$, i.e., electrons delocalize with increasing tunneling interaction. Spectral weights reflect this delocalization and measure the corresponding correlations in the system. If the interactions in the system are such that the system is strongly correlated, more states participate in the overlaps, but their contributions come with different phases. This gives rise to a strong suppression of the available transport channels, so that only a few contribute significantly to the current.

B. Current-voltage characteristics

We can use the values of the overlaps obtained in the previous section to calculate the current through the system as a function of gate voltage V_G and source-drain voltage bias $eV_{DS}=\mu_L-\mu_R$, via Eq. (4). V_{DS} is specified by the chemical potentials of emitter and collector electrodes, while sweeping the gate voltage V_G through positive values shifts down the electrostatic potential of the N-electron system in the DDS. For the symmetric case, we present in Fig. 5 results for the current for a range of values of interdot tunneling, in a gray-scale contour plot, where dark corresponds to small current (lighter shades indicate higher $|I|$ values, with sign equal to that of V_{DS}). The temperature for these calculations was set at $k_BT=0.01$ ($\simeq 120$ mK), an order of magnitude smaller than the mean level spacing. The general characteristics of these plots have been analyzed for single[13,36] and double[29] quantum dot systems. Notice that here we plot current, and not the differential conductance typically plotted, as a function of both V_G and V_{DS}, providing similar physical information (sample differential conductance traces are discussed below).

In these plots, the current in the linear regime, at $V_{DS}\simeq 0$ shows CB steps corresponding to changes in the ground state of the coupled dots from the N to the $N+1$ electron configuration (the ''addition spectrum''). The differential conductance traces would show CB peaks in the linear regime, separated by the actual charging energy required to add one electron to the system. As V_{DS} increases, excited states of both configurations become accessible near each CB peak, providing new tunneling channels through the double dot. This results in broadening of the CB peaks to form multiple peak structures enclosing ''Coulomb diamonds'' (appearing darkest in Fig. 5), corresponding to CB regions of zero conductance and fixed electron number, as indicated in each diamond. The lines defining the diamond edges correspond to transmission ''resonances'' or alignment of the ground states of the DDS with source or drain

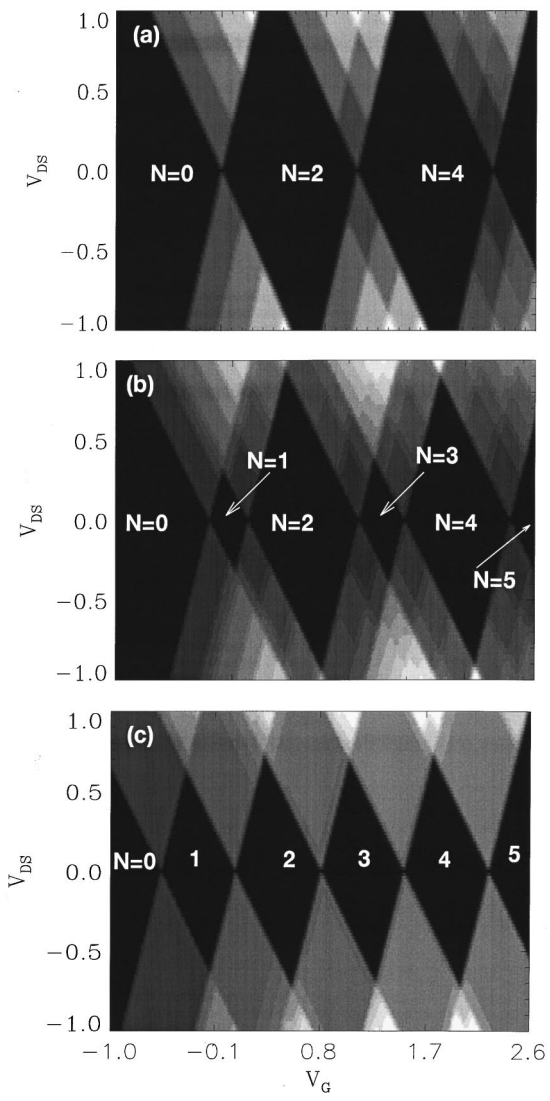

FIG. 5. Current as a function of gate voltage V_G and source-drain voltage V_{DS}, for different values of interdot tunneling: (a) $t=0.01$, (b) $t=0.1$, and (c) $t=0.2$. Symmetric DDS case.

Fermi levels. Lines parallel to the edges and away from the CB diamonds correspond to transitions involving excited states of the quantum molecule. For positive V_{DS}, we identify resonances parallel to the negative (or positive) slope Coulomb diamond edges as unoccupied DDS levels in resonance with the source (or drain) Fermi level, i.e., μ_L (or μ_R).

For the ideal symmetric double dot system for weak tunneling in Fig. 5(a), we obtain Coulomb blockade regions corresponding to ''even-even'' double-dot ground states in which each dot has the same number of electrons, and increasing the gate voltage adds electrons *in pairs* to the system, as the symmetric and antisymmetric quantum mechanical states are nearly degenerate for small t, and the local interaction dominates. The charging energy and corresponding CB diamonds are quite large (in comparison with those in other panels, see below). As t increases, Fig. 5(b), and the energy splitting between ground states becomes significant, we see that the current steps split, producing two different size diamonds. The smaller diamonds signal the N odd states, as one would expect that the split pairs in a bonding/

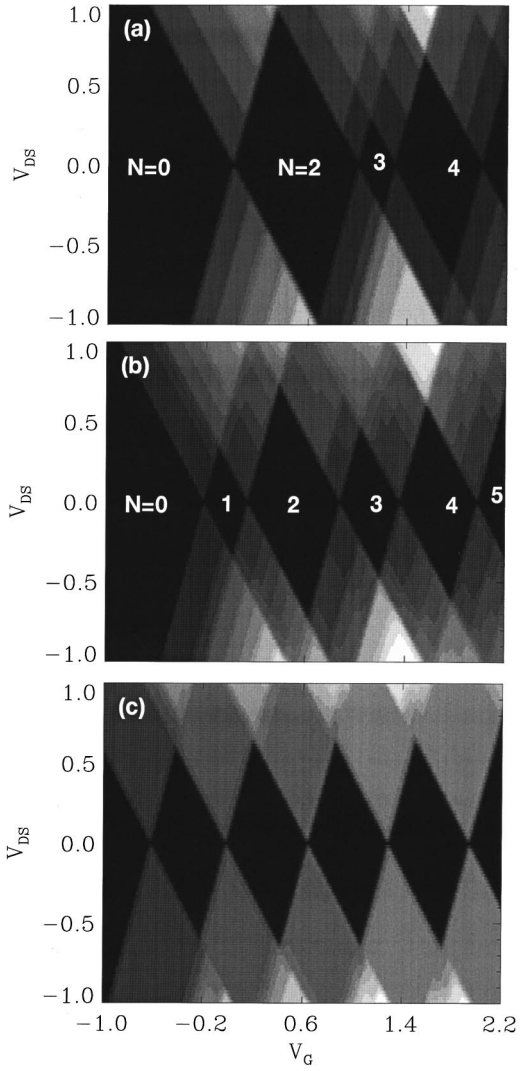

FIG. 6. Current in V_G-V_{DS} plane for asymmetric DDS. (a) $t=0.01$, (b) $t=0.1$, and (c) $t=0.2$. Notice asymmetry is nearly absent in (c) but still clearly seen in the finite bias current steps.

antibonding picture would be far away in energy from the next. This is intuitively expected for single-particle states mixed by a weak tunneling matrix element. That it is also the case for a multiparticle state with several local orbitals mixed in by tunneling and Coulomb interaction is a somewhat surprising result. Moreover, Blick *et al.* have shown that this mixing of many-particle ground states by parts is quite successful in describing experimental data in a double-dot geometry.[25]

As t increases further, the two types of diamonds are nearly identical [Fig. 5(c)], indicating that the states of the individual dots are fully mixed into an overall single dot with smaller charging energy (and then smaller CB diamonds) without any even-odd charging differentiation. Basically identical results have been nicely obtained in Ref. 31 by combining a two-site generalized Hubbard model with a one-dimensional step-well model for the confining double dot potential. Their calculated nonlinear transport characteristics are in excellent qualitative agreement with experiment by Crouch *et al.*,[29] for which they were designed.

In the case of asymmetric dots, recent experimental studies by Blick *et al.* have presented the charging diagram of

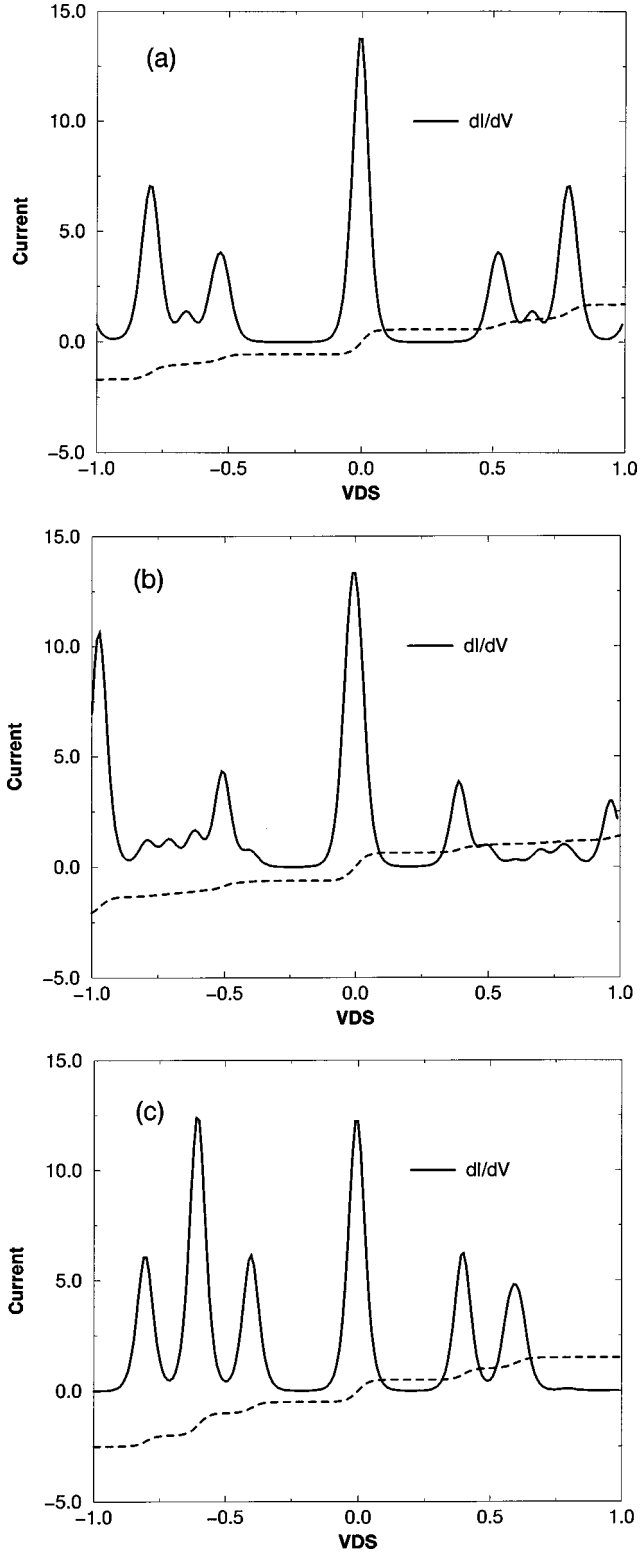

FIG. 7. Current and its derivative dI/dV_{DS} as a function of source-drain voltage V_{DS} for (a) symmetric $t=0.1$; (b) asymmetric $t=0.1$, and (c) asymmetric $t=0.01$ DDS. Gate voltages fixed as explained in text. Conductance peaks away from $V_{DS}=0$ are produced by a few of the excited states.

such series structure in the linear regime, as discussed above.[25] Our results for the asymmetric case (larger QD on the right) in the nonlinear regime, are shown in Fig. 6 again as a gray-scale contour plot of the current in the V_G-V_{DS}

plane. Here, we see a structure of small and large diamonds, even at $t \simeq 0$, which reflects the built-in asymmetry in the dots producing differences in charging energy from even to odd N, as opposed to the ideal symmetric case where we have full level degeneracy and charging by two electrons at a time [see Fig. 5(a)]. Also, note that I-V traces are *substantially* different depending on the *sign* of the polarization V_{DS}, since occupancy of states in the DDS in the collector side differs from that on the emitter side. Additionally, note that as in the symmetric case, small diamonds increase in size and width as interdot tunneling increases, since tunneling allows the extra electron to be shared between the two dots, and tends to effectively reduce the structural asymmetry. By the time $t=0.2$ in this asymmetric molecule, one can hardly distinguish the structural asymmetry any more, as shown in Fig. 6(c). The interdot tunneling has basically transformed the DDS into a single larger dot, with nearly identical CB diamonds for all N's *and* even similar excited-state structures.

From this discussion, it is clear that the most asymmetric situation occurs whenever the quantum dots making the molecule are not identical and the interdot tunneling is not too large. To further illustrate this, in Fig. 7 we plot the current and the differential conductance, dI/dV_{DS}, as a function of V_{DS}, for fixed values of the gate voltage V_G and interdot tunneling. In the symmetric case, Fig. 7(a), $V_G=1.09$ and $t=0.1$, while in the asymmetric cases, Figs. 7(b) and 7(c), $V_G=0.87$, $t=0.1$ and $V_G=1$, $t=0.01$, respectively.

These values of V_G are taken from Figs. 5 and 6, and correspond to the charging energy for the transition N: $2\rightarrow 3$.[37] The excited state symmetry is clearly observed in the curves shown for both the current and its derivative, as can be seen in Fig. 7(a). The central peak in differential conductance is the ground state to ground-state contribution, and is clearly the most important in all cases, although less so in the asymmetric structure. The lateral peaks correspond to the contributions from excited states, and we see that these start contributing at a smaller positive value of V_{DS} in the asymmetric case. Notice that the large feature in Fig. 7(b) at $V_{DS}\simeq -1$ corresponds to transitions involving the ground states N:$3\rightarrow 4$, which have become accessible at the finite bias. However, at $|V_{DS}|<1$, we see a number of transitions via excited states, some of which have quite a large value.

In the case of the effectively more asymmetric system, given its small value of interdot coupling $t=0.01$, the differential conductance is remarkably asymmetric, as shown in Fig. 7(c). The large feature at $V_{DS}\simeq -0.6$ is associated with the ground-state transition N:$3\rightarrow 4$ (just as above), while all the other smaller peaks are related to excited states: The feature at $V_{DS}\simeq -0.4$ is produced by an excited state of $N=3$ in the DDS, while that at $\simeq -0.8$ is via a $N=4$ excited configuration. On the other hand, the two differential conductance peaks for $V_{DS}>0$ are excited states of the $N=2$ configuration, which make quite a large contribution to the current and conductance. Notice that other transitions involving excited states [clearly seen in Fig. 7(b), or in the corresponding spectral weights] are suppressed here. Once again, this is consequence of the subtle wave function mixing that takes place for nonzero t. We should point out that although larger differences are apparent in Fig. 4 for the spectral weights for left- or right-incidence in asymmetric dots, this is not carried over as sharply in the current or conductance curves. Inspection of the symmetrized expression for the current, Eq. (4), suggests that the addition of the appropriate terms with Γ^L and Γ^R tends to deemphasize these differences.

IV. CONCLUSIONS

Using an extended Hubbard Hamiltonian, which takes into account intra- and interdot Coulomb interactions and variable interdot hopping, we calculate the overlap matrix elements $S^{L/R}_{\alpha\alpha'}$ and corresponding I-V characteristics for artificial diatomic molecules, in both symmetric and asymmetric geometries. The calculations are performed in the weak and strong tunneling regimes, as the number of electrons in the system increases from $N=0$, as a function of the gate voltage. The effects of interdot Coulomb interaction are found to be small and equivalent to a minor rescaling of the local intradot interaction, in agreement with Stafford *et al.*[20]

It is found in all cases that only a few of the many channels involving excited states of the DDS contribute to the current. In the symmetric case, the largest contribution corresponds to the channel involving the ground states of N and $N+1$ particles. Indeed, the contour diagrams of nonlinear current as a function of gate voltage V_G and source-drain voltage V_{DS} (Fig. 5) show the formation of primary and secondary diamonds (CB regions) evolving as interdot tunneling increases, in excellent qualitative agreement with experiments with nearly-identical coupled dots.[28,29] In the asymmetric case, with the largest dot on the right, we have to consider the difference in the overlaps $S^L_{\alpha\alpha'}$ and $S^R_{\alpha\alpha'}$ for incidence from left or right, respectively. In the *strong* tunneling regime, we find that in contrast to the symmetric case, there are several channels involving excited states that contribute to $S^L_{\alpha\alpha'}$. On the other hand, the main contribution to $S^R_{\alpha\alpha'}$ comes from the ground states of N and $N+1$ particles. From the behavior of the overlaps in this case we can say that the system is less correlated and that there are strong competing effects between tunneling coupling and asymmetry. These effects enter in the calculation of the current, and the final influence of excited states in the asymmetric case can best be appreciated in the diagrams for the current in the *weak* tunneling regime of Figs. 6(a) and 6(b) or 7(c). The experimental work by Blick *et al.*[25] on asymmetric double dot structures was concerned with the $V_{DS}=0$ regime. We believe that analysis of finite bias data in these structures should give unique insights into the dot molecular states, and encourage experimental groups to test asymmetric structures. Finally, a detailed theoretical analysis of the differential conductance as a function of ''back'' and ''top'' voltages, as defined in the split-gate experimental setup of Ref. 25 is possible with our present approach, and will be presented elsewhere.

ACKNOWLEDGMENTS

This work was supported in part by CONACYT Project No. 0078P-E9506 and DGAPA-UNAM Project No. IN100895. S.E.U. was supported in part by U.S. DOE Grant No. DE-FG02-91ER45334.

*Permanent address: Instituto Tecnológico de Tijuana, Centro de Graduados e Investigación, Apartado Postal 1166, Tijuana, B.C. 22000, Mexico.

[1] M. A. Kastner, Rev. Mod. Phys. **64**, 849 (1992); Phys. Today **46** (1), 24 (1993).

[2] R. C. Ashoori, Nature (London) **379**, 413 (1996); L. Kouwenhoven, Science **268**, 1440 (1995).

[3] J. H. F. Scott-Thomas, S. B. Field, M. A. Kastner, H. I. Smith, and D. A. Antoniadis, Phys. Rev. Lett. **62**, 583 (1989); U. Meirav, M. A. Kastner, and S. J. Wind, *ibid.* **65**, 771 (1990).

[4] D. V. Averin and K. K. Likharev, in *Quantum Effects in Small Disordered Systems*, edited by B. L. Altshuler, P. A. Lee, and R. A. Webb (Elsevier, Amsterdam, 1991).

[5] H. van Houten and C. W. J. Beenakker, Phys. Rev. Lett. **63**, 1893 (1989); C. W. J. Beenakker, H. van Houten, and A. A. M. Staring, *ibid.* **44**, 1657 (1991).

[6] Y. Meir, N. S. Wingreen, and P. A. Lee, Phys. Rev. Lett. **66**, 3048 (1991); Y. Meir and N. S. Wingreen, *ibid.* **68**, 2512 (1992).

[7] R. C. Ashoori, H. L. Störmer, J. S. Weiner, L. N. Pfeiffer, S. J. Pearton, K. W. Baldwin, and K. W. West, Phys. Rev. Lett. **68**, 3088 (1992).

[8] B. Meurer, D. Heitmann, and K. Ploog, Phys. Rev. Lett. **68**, 1371 (1992); D. Heitmann and J. P. Kotthaus, Phys. Today **46** (6), 56 (1993); M. Fricke, A. Lorke, J. P. Kotthaus, G. Medeiros-Ribeiro, and P. M. Petroff, Europhys. Lett. **36**, 197 (1996).

[9] S. Tarucha, D. G. Austing, T. Honda, R. J. van der Hage, and L. P. Kouwenhoven, Phys. Rev. Lett. **77**, 3613 (1996).

[10] D. G. Austing, T. Honda, K. Muraki, Y. Tokura, and S. Tarucha, Physica B **249-251**, 206 (1998).

[11] H. van Houten, C. W. J. Beenakker, and A. M. Staring, in *Single Charge Tunneling*, Vol. 294 of *NATO Advanced Studies Institute, Series B: Physics*, edited by H. Grabert and M. H. Devoret (Plenum Press, New York, 1991).

[12] C. W. J. Beenakker, Phys. Rev. B **44**, 1646 (1991).

[13] J. Weis, R. J. Haug, K. v. Klitzing, and K. Ploog, Phys. Rev. B **46**, 12 837 (1992); Phys. Rev. Lett. **71**, 4019 (1993).

[14] A. T. Johnson, L. P. Kouwenhoven, W. de Jong, N. C. van der Vaart, C. J. P. M. Harmans, and C. T. Foxon, Phys. Rev. Lett. **69**, 1592 (1992).

[15] E. B. Foxman, P. L. McEuen, U. Meirav, N. S. Wingreen, Y. Meir, P. A. Belk, N. R. Belk, M. A. Kastner, and S. J. Wind, Phys. Rev. B **47**, 10 020 (1993).

[16] P. L. McEuen, E. B. Foxman, J. M. Kinaret, U. Meirav, M. A. Kastner, N. S. Wingreen, and S. J. Wind, Phys. Rev. Lett. **66**, 1926 (1991); Phys. Rev. B **45**, 11 419 (1992).

[17] J. J. Palacios, L. Martin-Moreno, and C. Tejedor, Europhys. Lett. **23**, 495 (1993).

[18] D. Weinmann, W. Haüsler, and B. Kramer, Phys. Rev. Lett. **74**, 984 (1995).

[19] D. Pfannkuche and S. E. Ulloa, Phys. Rev. Lett. **74**, 1194 (1995).

[20] C. A. Stafford and S. Das Sarma, Phys. Rev. Lett. **72**, 3590 (1994).

[21] G. Chen, G. Klimeck, S. Datta, G. Chen, and W. A. Goddard III, Phys. Rev. B **50**, 8035 (1994).

[22] Z. M. Yu, T. Heinzel, and A. T. Johnson, Phys. Rev. B **55**, 13 697 (1997).

[23] N. C. van der Vaart, S. F. Godijn, Y. V. Nazarov, C. J. P. M. Harmans, J. E. Mooij, L. W. Molenkamp, and C. T. Foxon, Phys. Rev. Lett. **74**, 4702 (1995).

[24] F. R. Waugh, M. J. Berry, D. J. Mar, R. M. Westervelt, K. L. Campman, and A. C. Gossard, Phys. Rev. Lett. **75**, 705 (1995).

[25] R. H. Blick, R. J. Haug, J. Weis, D. Pfannkuche, K. von Klitzing, and K. Eberl, Phys. Rev. B **53**, 7899 (1996); R. H. Blick, D. Pfannkuche, R. J. Haug, K. von Klitzing, and K. Eberl, Phys. Rev. Lett. **80**, 4032 (1998).

[26] F. Hofmann, T. Heinzel, D. A. Wharam, J. P. Kotthaus, G. Böhm, W. Klein, G. Tränkle, and G. Weimann, Phys. Rev. B **51**, 13 872 (1995).

[27] A. S. Adourian, C. Livermore, and R. M. Westervelt, Superlattices Microstruct. **20**, 411 (1996).

[28] C. Livermore, C. H. Crouch, R. M. Westervelt, K. L. Campman, and A. C. Gossard, Science **274**, 1332 (1996).

[29] C. H. Crouch, C. Livermore, R. M. Westervelt, K. L. Campman, and A. C. Gossard, Appl. Phys. Lett. **71**, 817 (1997).

[30] R. H. Blick, D. W. van der Weide, R. J. Haug, and K. Eberl, Phys. Rev. Lett. **81**, 689 (1998).

[31] R. Kotlyar and S. Das Sarma, Phys. Rev. B **56**, 13 235 (1997).

[32] J. M. Kinaret, Y. Meir, N. S. Wingreen, P. A. Lee, and X.-G. Wen, Phys. Rev. B **46**, 4681 (1992).

[33] D. Pfannkuche and S. E. Ulloa, Adv. Solid State Phys. **35**, 65 (1996).

[34] T. H. Oosterkamp, S. F. Godijn, M. J. Uilenreef, Y. V. Nazarov, N. C. van der Vaart, and L. P. Kouwenhoven, Phys. Rev. Lett. **80**, 4951 (1998).

[35] F. Ramírez, E. Cota, and S. E. Ulloa, Superlattices Microstruct. **4**, 523 (1996).

[36] D. R. Stewart, D. Sprinzak, C. M. Marcus, C. I. Duruöz, and J. S. Harris, Jr., Science **278**, 1784 (1997).

[37] Notice that for the calculations in Fig. 7 we have used $\lambda = 1/2$ to study only the effects of the state symmetry and not those due to the asymmetry in potential drop across the DDS.